Robustness of Positional Specification by the Hedgehog Morphogen Gradient

David J Irons[1], Alexandre Wojcinski [2], Bruno Glise [2] , Nicholas A M Monk[3]

[1]School of Mathematics and Statistics, University of Sheffield, Sheffield, UK
[2]Centre de Biologie du Développement, UMR 5547 and IFR 109 CNRS/UPS, 118 route de Narbonne, 31062 Toulouse cedex 4, France
[3]School of Mathematical Sciences, University of Nottingham, Nottingham, UK

Abstract

Spatial gradients of Hedgehog signalling play a central role in many patterning events during animal development, regulating cell fate determination and tissue growth in a variety of tissues and developmental stages. Experimental evidence suggests that many of the proteins responsible for regulating Hedgehog signalling and transport are themselves targets of Hedgehog signalling, leading to multiple levels of feedback within the system. We use mathematical modelling to analyse how these overlapping feedbacks combine to regulate patterning and potentially enhance robustness in the *Drosophila* wing imaginal disc. Our results predict that the regulation of Hedgehog transport and stability by glypicans, as well as multiple overlapping feedbacks in the Hedgehog response network, can combine to enhance the robustness of positional specification against variability in Hedgehog levels. We also discuss potential trade-offs between robustness and additional features of the Hedgehog gradient, such as signalling range and size regulation.

Keywords: Hedgehog; Robustness; Feedback; HSPGs; Drosophila wing imaginal disc

Introduction

During the development of multi-cellular organisms, the spatial patterning of a wide range of tissues depends on the localised secretion of signalling factors (called morphogens) that move across the tissue to establish a spatial concentration gradient. These morphogen gradients are interpreted and modified by cellular signalling pathways in the responding tissue, where they regulate growth, gene expression and the eventual patterns of cell fate (Tabata and Takei (2004), Ashe and Briscoe (2006), Lander (2007), Jaeger et al. (2008)).

A remarkable feature of this process is the precision and robustness of the resulting patterns of cell fate in the face of fluctuations in protein levels and natural variability in the size and genetics of individuals. This prompts us to investigate the mechanisms that underlie properties such as robustness and size regulation. To this end, mathematical modelling can complement experimental results, providing a deeper understanding of the mechanisms behind these properties (Jaeger et al. (2008)). In this paper, we present a new mathematical model of Hedgehog (HH) gradient formation and signalling in the *Drosophila* wing imaginal disc, and use this to explore how the robustness of the positions of target gene expression boundaries is affected by

a range of experimentally observed mechanisms. The Hedgehog signalling pathway has been highly conserved during evolution, and plays a central role in the patterning of a range of tissues in both vertebrates and invertebrates (Ingham and McMahon (2001), Jia and Jiang (2006), Jiang and Hui (2008), Varjosalo and Taipale (2008)). Moreover, mis-regulation of the pathway is associated with a number of cancers and other human diseases (Mullor et al. (2002), Jiang and Hui (2008), Varjosalo and Taipale (2008)). Therefore, studying this system in the well characterised wing disc can provide insight into the development and mis-regulation of more complex tissues.

In the wing disc, HH is secreted by all cells of the posterior compartment, from where it moves into the anterior compartment, resulting in the formation of a stable posterior-to-anterior concentration gradient (Ingham and McMahon (2001), Jia and Jiang (2006), Callejo et al. (2006)). In signal-receiving cells in the anterior compartment, numerous target genes are expressed in response to different levels of HH signalling (Fig. 1A). The essential features of the Hedgehog signalling pathway are illustrated in Fig. 1B. HH binds to the transmembrane receptor Patched (PTC). When not bound by HH, PTC represses the activity of Smoothened (SMO), and consequently the remainder of the signalling pathway (including Costal2 (COS2) and Fused (FU)) promotes the phosphorylation and truncation of the transcription factor Cubitus interruptus (CI), yielding the repressive form CIR. However, on HH binding to PTC, the HH-PTC complex is internalised and degraded, releasing the inhibition of SMO, which can then recruit COS2 and FU. Phosphorylation of CI is consequently prevented, allowing the accumulation of the active form of CI (CIA). Target genes are regulated by both CIR and CIA at different thresholds. Important target genes include *decapentaplegic* (*dpp*), which encodes a second morphogen involved in anterior-posterior patterning and wing growth (Basler and Struhl (1994), Affolter and Basler (2007)), and *collier* (*col*), which plays an important role in wing vein positioning (Crozatier et al. (2003)).

Numerous factors are involved in regulating HH transport and signalling, many of which are themselves signalling targets (Fig. 1B). For example, *ptc* is a direct target of Hedgehog signalling (Chen and Struhl (1996)), and inhibition of SMO by PTC is antagonised by the bound HH-PTC complex (Casali and Struhl (2004)), leading to overlapping positive and negative feedback loops (Fig. 2). An analogous positive feedback loop also exists within the signalling pathway itself—Fused and Smoothened mutually promote each others activity and antagonise Patched function in response to high levels of signalling (Claret et al. (2007), Liu et al. (2007)).

An additional group of factors, which both regulate and are regulated by Hedgehog signalling, are Heparan sulfate proteoglycans (HSPGs), such as Dally and Dally-like (Dlp). Dally and Dally-like are both up-regulated in response to Hedgehog signalling, leading to a stripe of high expression (in each case) in anterior cells near the anterior-posterior border (Fujise et al. (2001), Crickmore and Mann (2007), Gallet et al. (2008)). This stripe overlaps with the Hedgehog signalling region and both proteins have been shown to influence the signalling pathway, in response to both high and low levels of Hedgehog (Callejo et al. (2006), Eugster et al. (2007), Gallet et al. (2008)). Moreover, Dally and Dally-like are involved in the transport of HH across the tissue (Han et al. (2004)), as well as in protecting it from degradation (Lin (2004), Bornemann et al. (2004), Callejo et al. (2006)). Changes to Hedgehog accumulation, transport and signalling range have also been observed in mutants that affect HSPG interactions or structure, such as *shifted* (Glise et al. (2005)), *tout velu* and *sister of tout-velu* (Bornemann et al. (2004)).

Many of the interactions and feedbacks identified in the wing disc also feature in the Sonic Hedgehog (Shh) signalling pathway in vertebrates. For example, Shh signalling results in the up-regulation of its receptor Ptc1 (Marigo and Tabin (1996)). Moreover, additional layers of regulation beyond those observed in *Drosophila* also exist. In particular, Shh signaling regulates a number of additional cell surface proteins that interact with and modulate the spread of Shh proteins across the tissue (Dessaud et al. (2008)).

Both experimental data and mathematical modelling suggest that regulative feedback and transport could play a central role in ensuring robustness and size-regulation in morphogen responses, in a range of developmental processes (Eldar et al. (2003), Ben-Zvi et al. (2008), Jaeger et al. (2008)). For example, in both *Drosophila* and *Xenopus* embryos, a combination of experimental and theoretical work has shown that the Bone Morphogenetic Protein (BMP) gradient—which patterns the dorso-ventral body axis—is robust against changes in the levels of important signalling factors and scales according to embryo size (Umulis et al. (2006), Ben-Zvi et al. (2008)). The models predict that this striking robustness depends on a combination of facilitated BMP transport and local regulation of BMPs in response to signalling. Mathematical modelling has also been used to investigate how HSPGs affect morphogen gradient formation and patterning, especially in relation to Wingless and Decapentaplegic signalling in the *Drosophila* wing (e.g. Hufnagel et al. (2006), Lander et al. (2007)).

In the context of patterning by Hedgehog gradients, previous theoretical work has investigated

how the up-regulation of *ptc* in response to Hedgehog signalling could enhance robustness to variations in Hedgehog production rate (Eldar et al. (2003)). In addition to *ptc* regulation, a number of other features of Hedgehog signalling in both vertebrates and invertebrates have been explored using mathematical models. Saha and Schaffer (2006) have produced a detailed model for Shh signalling in the vertebrate neural tube that incorporates both *ptc* up-regulation and Shh interactions with HSPGs and transmembrane proteins, such as Hhip and Dispatched. In the models, these interactions were shown to modify both the shape of the Shh gradient and the range of signalling, by regulating the rate of Shh movement and internalisation. Models have also been produced to investigate growth in the vertebrate limb bud (Dillon et al. (2003)) and bi-stability in Shh signalling in the vertebrate neural tube (Lai et al. (2004)). Moreover, Nahmad et al. (2008) have recently produced a model to investigate anterior-posterior wing disc patterning in *Drosophila* and ants, focusing on both Hh and Dpp signalling. Nahmad and Stathopoulos (2009) have also then gone on to investigate temporal effects on gradient formation and the eventual patterns of certain target genes. Existing models have been based predominantly on differential equations, but stochastic modelling (Lai et al. (2004)) and logical models (González et al. (2008)) have also been used.

This theoretical work has provided important insights into the function of certain interactions and model parameters. However, the roles of a number of experimentally observed mechanisms have yet to be investigated, and a complete understanding of the system is still lacking. In particular, how the multiple signalling components and feedbacks combine to regulate system properties such as robustness remains unclear. Furthermore, there is significant variability in parameter values between existing models, making it difficult to draw definite conclusions about the relative importance of different regulative mechanisms.

We have developed a new mathematical model for Hedgehog signalling in the *Drosophila* imaginal wing disc, focusing on the main regulatory interactions and feedbacks in the system. The model is simple enough to allow mathematical analysis and parameter estimation based on experimental data. Through the analysis of the gradients produced in this model, we explore the ways in which a number of experimentally observed interactions and feedbacks can combine to regulate the robustness of the spatial patterning of Hedgehog target gene expression. After demonstrating that wing patterning is in fact robust to changes in the rate of Hedgehog production, we use the model to investigate in detail how the positions of target gene expression boundaries respond to variability in Hedgehog production, stability and transport. We also

determine how these interactions affect the additional system-level properties of size-regulation and signalling range. Drawing on the strong similarities between the Hedgehog signalling pathway in different species, we also discuss how our results relate to more complex processes such as the patterning of the vertebrate neural tube by Shh.

Materials and Methods

A new mathematical model of Hedgehog gradient formation in the *Drosophila* wing imaginal disc

We have developed a new mathematical model for Hedgehog signalling in the *Drosophila* wing imaginal disc. Hedgehog protein (HH) is produced in all cells of the posterior compartment and moves within the tissue, establishing a spatial concentration gradient in the anterior compartment. Experimental evidence indicates that the principal determinant of Hedgehog signalling is position along the anterior-posterior axis of the disc. We therefore neglect any dependence on dorso-ventral position and study a one-dimensional anterior-posterior cross section across the disc. We denote position along the anterior-posterior (AP) axis by x, such that $-L_A \leq x \leq L_P$, $x = 0$ corresponds to the AP boundary, and L_A and L_P are the lengths of the anterior and posterior compartments, respectively. Our one-dimensional domain is similar to those used in previous models of gradient formation (e.g. Lander et al. (2002), Eldar et al. (2003), Hufnagel et al. (2006), Lander et al. (2007)). Since HH is produced only in posterior compartment cells, and the signalling pathway is active only in anterior compartment cells, the model equations take distinct forms on the two sides of the AP compartment boundary.

The dynamics of the model variables $V(x,t)$ are represented by deterministic differential equations that model how the concentration or activity levels $[V]$ vary over time (t) and space (x). For simplicity, we do not include mRNAs explicitly, focusing rather on key proteins and protein complexes. Moreover, we represent the central uni-directional section of the Hedgehog signalling cascade (including SMO and CI—see Fig. 1B), by a single variable S corresponding to 'signalling response'. These simplifications do not affect the forms of the key feedbacks and transport mechanisms that are the main focus of this paper, but do reduce the number of model parameters and facilitate analysis of the model.

The key features incorporated in the model are as follows

1. HH is secreted at a rate ρ_h by all cells of the posterior compartment.
2. HH exists in two forms: 'free' (HH_f) and 'bound to HSPG' (HH_b). This allows us to explore the roles of HSPGs in binding, transporting and stabilising HH.
3. Free and bound HH diffuse with diffusion coefficients D_f and D_b, respectively.
4. Free and bound HH are degraded with linear rates γ_f and γ_b, respectively.
5. HH and HSPGs bind and unbind at rates k_{out} and k_{in}, respectively. The amount of bound HH is limited by the amount of HSPGs, and saturates at a level μ.
6. In the anterior compartment, HH_b binds/unbinds to Patched (PTC) to form HH-PTC complex (PH) at rates k_{on} and k_{off}, respectively.
7. PH is internalised (and subsequently degraded) at rate γ_{ph}.
8. The level for activity of the signalling pathway is represented by S. Signalling activity is repressed by PTC, and this repression is antagonised by PH. To represent this antagonism, we introduce the variable $[Z] = \dfrac{[PTC]}{1 + r[PH]}$ to represent 'active PTC' (which is bounded above by $[PTC]$). r represents the strength of PH antagonism: $1/r$ is the level of $[PH]$ at which PTC repression of S is reduced by half. Repression of S by Z is represented by a monotonic decreasing function $g_s([Z])$ (see below for example).
9. PTC and HH target genes are up-regulated in response to S, represented by monotonic increasing functions $f([S])$ (see below for example).
10. Production/activation and linear degradation rates of all protein and complexes are represented by ρ and γ, respectively.

These features are encoded in the following differential equations, with individual parameters described in Table 1:

Posterior cells: $x \in (0, L_P)$

$$\frac{\partial [HH_f]}{\partial t} = \rho_h + D_f \frac{\partial^2 [HH_f]}{\partial x^2} - k_{out}[HH_f]\,(\mu - [HH_b]) + k_{in}[HH_b] - \gamma_f [HH_f] \quad (1)$$

$$\frac{\partial [HH_b]}{\partial t} = D_b \frac{\partial^2 [HH_b]}{\partial x^2} + k_{out}[HH_f]\,(\mu - [HH_b]) - k_{in}[HH_b] - \gamma_b [HH_b] \quad (2)$$

Anterior cells: $x \in (-L_A, 0)$

$$\frac{\partial [HH_f]}{\partial t} = D_f \frac{\partial^2 [HH_f]}{\partial x^2} - k_{out}[HH_f]\,(\mu - [HH_b]) + k_{in}[HH_b] - \gamma_f [HH_f] \quad (3)$$

$$\frac{\partial [HH_b]}{\partial t} = D_b \frac{\partial^2 [HH_b]}{\partial x^2} + k_{out}[HH_f]\,(\mu - [HH_b]) - k_{in}[HH_b] - k_{on}[HH_b][PTC] + k_{off}[PH] - \gamma_b [HH_b] \quad (4)$$

$$\frac{\partial [PTC]}{\partial t} = \rho_{p1} + \rho_{p2} f_p([S]) - k_{on}[HH_b][PTC] + k_{off}[PH] - \gamma_p [PTC] \quad (5)$$

$$\frac{\partial [PH]}{\partial t} = k_{on}[HH_b][PTC] - k_{off}[PH] - \gamma_{ph}[PH] \quad (6)$$

$$\frac{\partial [S]}{\partial t} = \rho_s g_s([Z]) - \gamma_s [S] \quad (7)$$

$$\frac{\partial [Gene]}{\partial t} = \rho_g f_g([S]) - \gamma_g [Gene], \quad (8)$$

where $[Z] = \dfrac{[PTC]}{1 + r[PH]}$ and $[Gene]$ represents a generic target of Hedgehog signalling.

HSPG up-regulation in response to signalling can be incorporated in the model by allowing the parameters μ, D_b and k_{on} to vary in response to signalling. For example, the effects of taking k_{on} to be a function of $[S]$ are discussed below.

Published experimental data and model approximations were used to generate reasonable estimates of (or constraints on) the values of the main model parameters (see Table 1 and **C1-C10** in *Supporting Text*). This process required specification of the (relative) levels of HH_b at the posterior margin (μ) and the anterior-posterior boundary (α_0), and of the value of Z at the Patched production boundary (z_A). The issue of parameter estimation is addressed in the *Discussion*.

In order to obtain approximate analytic expressions for different sections of the HH_b gradient, two reduced models were derived (Models B and C in *Supporting Text*). These approximations were used to derive Eqns. (9)–(17) below. Comparisons of the steady-state gradients generated by these approximations and by the full model are shown in *Supporting Figure* S16.

Model non-dimensionalisation

The model is non-dimensionalised by scaling all variables by the levels of PTC at the anterior margin, where there is little Hedgehog signalling (given by $\frac{\rho_{p1}}{\gamma_p}$). Distance is scaled by the average cell diameter $w \approx 2.6\mu m$ (Kicheva et al. (2007)), and time by the half-life of PTC. Specifically, we set

$$[V] \to [V]\frac{\gamma_p}{\rho_{p1}},$$
$$t \to t\gamma_p,$$
$$x \to \frac{x}{w},$$

for each model variable $[V]$.

Parameters are scaled as follows: $\rho_i \to \frac{\rho_i}{\rho_{p1}}$, $\gamma_i \to \frac{\gamma_i}{\gamma_p}$, $D_i \to \frac{D_i}{\gamma_p w^2}$, $k_{on} \to k_{on}\frac{\rho_{p1}}{\gamma_p^2}$, $k_{off} \to \frac{k_{off}}{\gamma_p}$, $k_{out} \to k_{out}\frac{\rho_{p1}}{\gamma_p^2}$, $k_{in} \to \frac{k_{in}}{\gamma_p}$, $\mu_i \to \mu_i\frac{\gamma_p}{\rho_{p1}}$, $r \to r\frac{\rho_{p1}}{\gamma_p}$.

How these non-dimensionalised parameters correspond to real parameters is revisited in the *Discussion*.

Functions used during analysis and simulations

The full model (Eqns. (1)–(8)) includes increasing and decreasing functions (f_i and g_i) to represent the rate of production of regulated variables. In simulations, we use sigmoidal Hill functions:

$$f_i(x) = \frac{x^{n_i}}{x^{n_i} + {c_i}^{n_i}},$$
$$g_i(x) = \frac{{c_i}^{n_i}}{x^{n_i} + {c_i}^{n_i}},$$

where x is the input concentration for function i, c_i is the activation / inhibition threshold and n_i encodes the steepness (cooperativity) of regulation about the threshold. The values of c_i and n_i used for PTC and S regulation are given in Table 1. For PTC regulation, we use a relatively steep function ($n_p = 8$), since the threshold $c_p = 0.72$ is quite close to 1 and a large n_p is necessary to achieve a maximum response ($f_p \approx 1$) when signalling S is high.

Since this model simplifies the main signalling cascade into a single variable, these Hill functions provide a way of accounting for any non-linear responses in the signalling pathway. Moreover, non-linearity (setting $n_p = 8$) provides a good fit to the Patched profiles reported in Casali and Struhl (2004). The results of simulations using either $n_p = 4$ or linear production functions are shown in *Supporting Figures* S10–S13 and demonstrate that there is no qualitative difference.

To represent the dependence of HH transport, stability and signalling on HSPG levels, relevant parameters take compartment-specific values. As a simplification, we assume that parameter values are spatially uniform within each compartment. However, to represent the effect of HSPG regulation (via signalling) on the binding rate of HH and PTC (k_{on}), we use a function of the form

$$k_{on}([S]) = k_{on}\left(1 + 4\frac{[S]^n}{[S]^n + c^n}\right).$$

When deriving Eqns. (13)–(15), we make a number of simplifications to facilitate mathematical analysis. One important simplification is the use of a step function representation of the function f_p that represents the Patched production rate. Thus, we assume that $f_p = 0$ if $[S] < c_p$ and $f_p = 1$ if $[S] \geq c_p$. This is roughly equivalent to letting $n_p \to \infty$ in the Hill function representation. The derivations themselves are described in *Suppporting Text* (Model C).

Experimental procedures

Drosophila strains

The following strains were used: Oregon-R, a natural population used as wild-type (*wt*) and ry^{506}, hh^{AC}/TM6B,Tb1 hh^{AC} being an amorphic allele which removes the *hh* promoter and part of the coding region (Lee et al. (1992)).

Immunohistochemistry and images capture

Discs were fixed in 4% paraformaldehyde in phosphate-buffered saline (PBS) for 20 min. To reduce background staining, tissues were incubated one hour in PAT (PBS containing 1% Tween 20 and 0.1% BSA). Incubation with primary antibody was carried out overnight at 4 °C in PAT

using a mouse anti-Col antibody, 1:50 (Dubois et al. (2007)), followed by fluorescent secondary antisera. Imaginal discs were mounted in polyvinyl alcohol 4-88 (Fluka) and observed with Leica SP5 confocal microscope. Captured images were assembled with Adobe Photoshop.

Results

Robustness of wing patterning in response to changes in Hedgehog production

Since many factors can affect Hedgehog production by posterior compartment cells (such as gene dosage, stochasticity in gene expression, or epigenetic factors), a key question is how regulatory interactions in the Hedgehog signalling pathway ensure robustness of boundaries of target genes expression despite such variability.

To demonstrate that patterning is indeed robust to variations in Hedgehog production, we have analysed the wing phenotype of adult flies where the production of Hedgehog is challenged by removing one copy of the *hh* gene. We focused particularly on the presence and position of the adult longitudinal veins (L2 to L5) which are highly stereotypically patterned in response to Hedgehog dependent secondary signals (Blair (2007)). To perform this analysis, we used a *Drosophila* stock carrying the hh^{AC} null allele, where the *hh* promoter and part of the coding sequence were removed (Lee et al. (1992)), over the TM6B balancer chromosome. We then out-crossed this stock with wild-type Oregon-R flies and analysed the wing phenotypes of all the $hh^{AC}/+$ and TM6B/+ adults emerging from this cross (Fig. 3). All the TM6B/+ wings analysed (n=252) were wild-type. Of all the $hh^{AC}/+$ wings analyzed (n=422), the majority of the wings present no mutant phenotype (Fig. 3A), but around 5% of the wings (n=19) show a slight disruption of the tip of L5 vein (Fig. 3B). This defect is reminiscent of phenotypes observed in some mutant alleles of the Hedgehog canonical transcription factor encoding gene *cubitus interruptus* (*ci*) (Slusarski et al. (1995)). However, we never observed any modification of the positioning of veins L3 and L4 in adult $hh^{AC}/+$ wings, which is a sensitive and direct read-out of Hedgehog activity in the wing. Indeed, the L3–L4 vein spacing is precisely defined by Hedgehog signalling through the activation of the Collier (Col) transcription factor during third instar larval stage. Subsequently, Collier specifies the presumptive L3–L4 intervein domain in a cell autonomous manner but also contributes to the induction of L3 and L4 provein cells in adjacent

domains (Crozatier et al. (2002)). To further confirm the absence of an L3–L4 patterning defect in heterozygous *hh* flies, we analysed Collier expression in late third instar wing imaginal discs from wild-type (*wt*) or $hh^{AC}/+$ flies (Fig. 3D-E). We were unable to visualise any modification of the number of cells activating Collier along the Anterior-Posterior (AP) axis (Fig. 3F). Taken together, these results confirm the robustness of Hedgehog signalling to changes in the HH production rate during *Drosophila* wing development.

Identification of mechanisms associated with robustness to changes in Hedgehog levels

In order to investigate the question of robustness, mathematical modelling can be used as a tool to supplement existing data on this system and provide predictions for future work. Below, we analyse the steady state behaviour of our mathematical model to predict mechanisms which could enhance the robustness of target gene expression boundaries against individual variability. In our model, we assume that HH acts as a morphogen in the anterior compartment such that the expression boundaries of the targets (e.g. *col*,*dpp*) occur at specific threshold levels of activity. Our initial and main focus is then on the sensitivity (robustness) of the position of target gene expression boundaries to changes in HH levels (both in terms of the rate of production of HH in the posterior compartment and the level of HH at the anterior-posterior (AP) boundary).

Towards these aims, we use the model to derive approximations for key aspects of the gradient, in terms of the model parameters (Eqns. (10)–(15) and (17); described in Fig. 1 and Table 1). For example, HH levels at the AP boundary (α_0) and the boundary of high *ptc* expression (α_A at position x_A), as well as the point at which HSPG saturation occurs (x_P) can be used to investigate how different interactions and mechanisms affect properties of positional signalling such as robustness.

Regulated transport and stability can enhance robustness to variations in Hedgehog production

HSPGs are believed to play a role in both the stabilisation and transport of morphogens (e.g. Callejo et al. (2006), Gallet et al. (2008)). To investigate the effect of HSPGs in the posterior compartment (where Hedgehog is produced) we compare our full model to a 'free diffusion'

model that ignores the roles of HSPGs (by changing appropriate parameters in the model). Fig. 5 illustrates our finding that interactions between HSPGs and HH in the posterior compartment can lead to enhanced robustness of target gene positioning in response to variations in HH production (red vs black dashed lines in Fig. 5B,C). This is demonstrated by a reduced shift in target gene boundary position in response to changes in HH production ρ_h. However, enhanced robustness is only evident once a critical threshold of HH production has been surpassed, corresponding to the point where HSPGs become saturated with HH at the posterior margin (diamond in Fig. 5C).

To understand the origin of this effect, we developed a simplified 'regulated transport' model (Model B in *Supporting Text*) and compared this to a 'free diffusion' model (Model A in *Supporting Text*) which does not include the effects of HSPGs. To facilitate mathematical analysis, we assumed that the HH diffusion/transport rate $D_b(i)$ and HH degradation rate $\gamma(i)$ depend on the compartment (i = A or P), but that any dependence of these parameters on HSPG levels or signalling is uniform across each of the compartments. At least in posterior cells (of primary interest below), this is appropriate, since the data indicate that these effects are not strictly dose dependent. Indeed, transport in discs mutant for only one of the HSPGs *dally* or *dlp* are relatively normal (Han et al. (2004), Eugster et al. (2007)).

Using the simplified models, we can then derive approximations for (i) the HH concentration at the AP boundary (α_0), and (ii) the target gene expression boundary (x_T), in terms of the HH production rate ρ_h:

Model A: Free Diffusion

$$\alpha_0 = \frac{\rho_h}{\gamma(P)} \left(\frac{\tanh\left(\frac{L_P}{\lambda_P}\right)}{\frac{D_b(A)}{D_b(P)}\frac{\lambda_P}{\lambda_A} + \tanh\left(\frac{L_P}{\lambda_P}\right)} \right) \tag{9}$$

Model B: Regulated Transport

$$\alpha_0 = \begin{cases} \dfrac{\rho_h \lambda_A L_P}{D_b(A)}, & \text{if } x_P > L_P \\ \dfrac{\rho_h \lambda_A^2 D_b(P)}{D_b(A)^2}\left(-1+\sqrt{1+\dfrac{2\mu D_b(A)^2}{\rho_h \lambda_A^2 D_b(P)}}\right), & \text{if } x_P < L_P \end{cases} \tag{10}$$

where $\lambda_i = \sqrt{\dfrac{D_b(i)}{\gamma(i)}}$ for $i =$ A or P, is the diffusion wavelength associated with each compartment, and

$$x_P = \lambda_A \frac{D_b(P)}{D_b(A)}\left(-1+\sqrt{1+\frac{2\mu D_b(A)^2}{\rho_h \lambda_A^2 D_b(P)}}\right) \tag{11}$$

is the posterior compartment position at which HSPGs become saturated with HH (see *Supporting Text* for derivations).

By assuming an approximately exponential gradient $\left(\alpha_0 \exp -\dfrac{|\, x\,|}{\lambda_A}\right)$ in the anterior compartment for both models, the position of the target gene expression boundary (corresponding to a HH concentration $[HH_b]_T$) can then be approximated as

$$x_T = \lambda_A \ln\left(\frac{\alpha_0}{[HH_b]_T}\right). \tag{12}$$

To consider the robustness of this boundary position in response to changes in the HH production rate ρ_h, we first derive expressions for the sensitivity coefficient $\sigma \equiv \dfrac{\partial x_T}{\partial \rho_h}$. For Model A, $\sigma = \dfrac{\lambda_A}{\rho_h}$, whereas for Model B,

$$\sigma = \begin{cases} \dfrac{\lambda_A}{\rho_h}, & \text{if } x_P > L_P \\ \dfrac{\lambda_A}{\rho_h} - F(\rho_h), & \text{if } x_P < L_P, \end{cases}$$

where $F(\rho_h) > 0$ (proved in Result S6 of *Supporting Text*). Thus, if the rate of Hedgehog production in Model B is above a critical value at which binding to HSPGs begins to saturate within the posterior compartment (so $x_P < L_P$), the sensitivity coefficient is lower than in Model A. Thus, our model precictes that interactions between HH and HSPGs can increase the robustness of positional specification in the anterior compartment, for sufficiently high levels of

HH production in the posterior compartment.

To determine the extent of this enhanced robustness, we consider the effect of a change in HH production rate from ρ_h to $\rho'_h = c\rho_h$. In line with the above sensitivity results, two distinct behaviours can be observed in the models, when looking at the corresponding shifts in the level of HH at the AP boundary (α_0 to α'_0).

In Model A, it is clear that $\alpha'_0 = c\alpha_0$ and $x'_T = x_T + \lambda_A \ln c$. This is also true for Model B when both x_P and x'_P (the HSPG saturation position when the production rate is ρ'_h) both exceed L_P (i.e. HSPG does not saturate within the posterior compartment). However, in Model B when both x_P and x'_P are less than L_P, we can can show that α'_0 does not shift as far as $\sqrt{c}\alpha_0$ (proved in Result S7 of *Supporting Text*). Specifically,

- if $c \geq 1$, then $\alpha_0 \leq \alpha'_0 \leq \sqrt{c}\alpha_0$ and $x_T \leq x'_T \leq x_T + \lambda_A \ln \sqrt{c}$,
- if $c \leq 1$, then $\alpha_0 \geq \alpha'_0 \geq \sqrt{c}\alpha_0$ and $x_T \geq x'_T \geq x_T + \lambda_A \ln \sqrt{c}$.

These bounds (for α_0) are illustrated as the shaded regions in Fig. 5A. Clearly, if the change in ρ_h is such that x_P passes L_P (e.g. if $x'_P < L_P < x_P$), then an intermediate shift in x_T results.

Therefore, once the rate of morphogen production ρ_h passes a critical point such that $x_P = L_P$ (represented by the diamond in Fig. 5C), the system containing HSPGs becomes more robust. There is a significant increase in robustness so that a c-fold increase in production only leads to a $\sqrt{c}$-fold change (or better) in the concentration of HH at the AP boundary and a $\lambda_A \ln \sqrt{c}$ shift (or better) in the position of the target gene expression boundary (black dotted line in Fig. 5C). This is opposed to a c-fold change and a $\lambda_A \ln c$ shift in the free diffusion model (black dashed line in Fig. 5C). Since the approximation in Model B depends on a large value for k_{out} compared to γ_f, we repeated the above simulations for a lower value of k_{out} and an increased value of γ_f. The theoretical predictions still hold (*Supporting Figure* S3).

In our model, the principal origin of this robustness is a restriction in the amount of HH that can be stably held in complex with HSPGs at the cell surface (μ). This in turn restricts the amount of HH that can travel to anterior cells. Adding this restriction mechanism leads to the existence of a critical posterior position ($x_P = L_P$) at which HSPGs become saturated at the posterior margin. Indeed, without this restriction mechanism, other potential HSPG-mediated functions (transport, stability) can not account for the same robustness (*Supporting Figure* S4). As can

be seen from the equation for x_P (Eqn. (11)), a number of variables affect the rate of production of HH at which this critical point (and hence the phase of enhanced robustness) is reached. These include the diffusion rate D_b, the HSPG binding capacity μ, and the "wavelength" of the anterior gradient λ_A. However, once the threshold rate of HH production has been passed, changes to these parameters have relatively little additional effect on robustness (results not shown).

In our regulated transport model, we have assumed that HSPGs play a role in both stabilising HH and in restricting the amount of HH that can be held at the cell surface. As can be seen in Fig. 5D, this stabilisation has an additional effect (red vs blue lines), above and beyond that produced by restricting the amount of HH held at the surface (blue vs black dashed line). Therefore, both of these mechanisms play an important role in enhancing robustness.

Multiple feedbacks combine to regulate Patched and can enhance robustness to variations in Hedgehog levels

Both the presence of negative feedback loops in signalling response networks and regulation of receptor levels by signalling activity have previously been associated with enhanced robustness (e.g. Eldar et al. (2003), Jaeger et al. (2008)). Since both are involved in Patched regulation, we next look in more detail at this aspect of the Hedgehog response. To separate the effects of regulation in the anterior compartment from the transport mechanisms discussed in the previous section, we consider a model comprising only anterior compartment cells and assume a fixed level of HH_b at the AP boundary (α_0), as in Fig. 4.

In the *Drosophila* wing imaginal disc, at least three overlapping feedback loops combine to regulate Patched levels and signalling in response to Hedgehog signalling (see Fig. 2). In order to test the potential effects of these feedbacks on robustness, we vary or modify three relevant parameters:

1. ρ_{p2}**:** the strength of Patched up-regulation in response to signalling,
2. r**:** the strength of antagonism of the inhibitory effect of PTC by the HH-PTC complex,
3. k_{on}**:** the rate of HH-PTC binding and internalisation (dependent on the levels of signalling and HSPGs).

For ρ_{p2} and r, we simply increase the values of the parameters from 0 to the estimated values in Table 1 (36 and 0.8 respectively). We make k_{on} an increasing function of Hedgehog signalling, so that it can increase up to 5-fold near the AP border (see *Materials and Methods*). This up-regulation of k_{on} in response to signalling is used to model the effect of up-regulating HSPGs (in particular Dally-like) in response to high levels of Hedgehog signalling.

As can be seen in Fig. 6A, each additional feedback leads to enhanced positional robustness of target gene boundaries in response to variations in HH levels at the AP boundary (in the model). This is demonstrated by a reduced shift in target gene boundary position in response to changes in HH levels α_0. The addition of negative feedback via ρ_{p2} has the largest effect on robustness (blue vs green line). Addition of either of the two positive feedbacks, via r and k_{on}, leads to a further enhancement in robustness (red and dashed black vs blue respectively). To allow direct comparison, the models were matched so that HH levels were equal at the AP boundary, but HH levels differed at the target gene boundary (see Fig. 4A). In order to ensure these results were not an artefact of this matching, we also modified the models to ensure HH levels were equal at the target gene boundary and obtained qualitatively similar results (Fig. 6B and *Supporting Figure* S5). We also repeated the simulations for the full posterior-anterior model with changes in the HH production rate (ρ_h) (Fig. 6C and *Supporting Figure* S6).

This robustness can be explained in terms of the Patched producing region and the magnitude of the Hedgehog gradient close to the AP boundary (where $[HH_b] = \alpha_0$). If $[HH_b]$ at the AP boundary increases from α_0 to $c\alpha_0$, then the distance from the boundary at which $[HH_b]$ falls back to α_0 (x_c, say) will decrease as the gradient steepens. Beyond this point, the steady-state gradient will be a copy of the original, but shifted away from the boundary by distance x_c.

To approximate the magnitude of the gradient at the AP boundary, we first consider the high Patched production region close to the AP boundary. Using a model approximation (Model C in *Supporting Text*), the HH threshold corresponding to high Patched production (α_A) and the corresponding boundary position (x_A) are given below and shown in Fig. 1A:

$$\alpha_A = \frac{(\rho_{p1}+\rho_{p2}-\gamma_p z_A)(\gamma_{ph}+k_{off})}{(\gamma_{ph}+r(\rho_{p1}+\rho_{p2}))k_{on}z_A}, \tag{13}$$

$$x_A = \frac{D_b}{\rho_{p1}+\rho_{p2}}\left(\sqrt{\frac{2(\rho_{p1}+\rho_{p2})}{D_b}(\alpha_0-\alpha_A)+\left(\frac{\alpha_A}{\lambda_A}\right)^2}-\frac{\alpha_A}{\lambda_A}\right), \tag{14}$$

where z_A is the value of $[Z]$ corresponding to the Patched production threshold and $\lambda_A = \sqrt{\frac{D_b}{\delta k_{on}}}$ (see Model C in *Supporting Text* for derivations). Here, δ is an approximation of $[PTC]$, anterior of the high Patched-production boundary x_A. Suitable bounds for δ are derived in *Supporting Text* (Model C; Eqn. (18)).

Then (as derived in Model C of *Supporting Text*), the magnitude of the gradient in $[HH_b]$ at the AP boundary is given by

$$g = \begin{cases} \alpha_0\sqrt{\frac{\delta k_{on}}{D_b}}, & \text{if } \alpha_0 < \alpha_A \\ \sqrt{\frac{2(\rho_{p1}+\rho_{p2})}{D_b}(\alpha_0-\alpha_A)+\frac{\delta k_{on}\alpha_A^2}{D_b}}, & \text{if } \alpha_0 \geq \alpha_A. \end{cases} \tag{15}$$

As proved in Result S12 of *Supporting Text*, g increases (or remains unchanged) if either (i) α_A decreases due to a single parameter change (excluding ρ_{p1} or ρ_{p2}) or (ii) the transport rate D_b decreases. Therefore, parameter changes that lead to a decrease in α_A lead to an increase in the gradient at the AP boundary and an increase in robustness. Returning to the results in Fig. 6, the values for α_A and g can be seen in Table 2 for the different parameter sets. Increasing k_{on} or r close to the source leads to a sharp drop in α_A, which shifts the system from moderate Patched up-regulation (if $\alpha_A > \alpha_0$) to high Patched up-regulation (if $\alpha_A < \alpha_0$), and leads to a steeper Hedgehog gradient and enhanced robustness. This implies that more Patched is produced close to the source and more HH is removed from the surface, resulting in a steeper gradient and enhanced robustness. Further reductions in α_A (once $\alpha_A \leq \alpha_0$) have a smaller effect.

Increasing Patched production (ρ_{p1}, ρ_{p2}) generally leads to an increase in the gradient at the AP boundary and increased robustness. The above mentioned increase in robustness (blue vs green lines) can be attributed to an increase in ρ_{p2}, leading to an increase in $\delta(\equiv [Ptc]$ levels)

and g.

In the simulations shown in Fig. 6A,C, the models were matched so that HH levels at the AP boundary (α_0) equal 10. When we repeated the simulations, matching at a lower $\alpha_0 = 5$ (*Supporting Figure* S5 and S6), we found larger differences between the above models (red and black dashed vs blue lines). Returning to Table 2, this makes sense since the case when $\rho_{p2} = 36$, $r = 0$ and $k_{on} = 8$ (blue model) is further away from high Patched production, whilst the models with additional feedbacks still lead to maximum Patched production at the AP boundary.

Here, we have focussed on the feedbacks that directly affect the Hedgehog receptor Patched. However, additional feedbacks also exist within the signalling pathway, such as a positive feedback between Smoothened and Fused that antagonises Patched function in response to high Hedgehog signalling (Claret et al. (2007), Liu et al. (2007)). As can be seen in *Supporting Figures* S14 and S15, this feedback has the same effect as the two positive feedbacks discussed above—Patched up-regulation is enhanced close to the AP boundary, leading to an enhancement in robustness to variations in HH levels. Indeed, this is generally the case when a positive feedback antagonises the negative feedback loop up-regulating Patched.

As mentioned above, other parameters (such as D_b) can also affect robustness by regulating the steepness of the gradient. This is particularly interesting since HSPGs are believed to play a role in morphogen transport and so this could provide an additional mechanism by which they could enhance robustness. A decrease in the HH transport rate close to the source due to HSPGs or signalling can have a similar effect to an increasing k_{on}. This ability to increase robustness through reduced diffusion has also been proposed by other authors (Bollenbach et al. (2007)).

Robustness in response to parameter variations

Both intrinsic and extrinsic variability of model parameters could lead to changes and fluctuations that also affect boundary positions. We therefore examine positional robustness to changes in value of a range of parameters in both posterior and anterior compartments.

With respect to anterior parameters, the models are most sensitive to changes in the HH diffusion/transport rate (D_b) and in the rate of HH-PTC binding (k_{on}), with target gene boundaries shifting significantly in response to changes in these parameters (Fig. 7A,B and *Supporting Fig-*

ure S7). In both these cases, the target gene boundary is also more sensitive when there are feedbacks regulating Patched production (Fig. 7A,B, green vs blue, red and black dashed lines). As can be seen in Fig. 7C,D, different feedbacks can affect a parameter in different ways. Here, parameters involved in Patched up-regulation lead to opposite shifts in the target gene boundary when we consider models involving Patched antagonism r (red) and k_{on} regulation (black dashed line). A model that incorporates both feedbacks can maintain a similar shaped gradient, thus counteracting some of this variability (black dotted line).

Interestingly, feedback in anterior cells can have a positive impact on positional robustness to changes in several posterior parameters (Fig. 7E,F and *Supporting Figure* S8). This is particularly evident for sensitive parameters such as the HH diffusion/transport rate D_b and HH-HSPG binding (k_{out}) (Fig. 7E,F). Therefore, it appears that sharpening the anterior gradient can make the system more robust to the secretion and transport of Hedgehog in posterior source cells.

Discussion

We have demonstrated experimentally that patterning in response to Hedgehog signalling is robust against variability in Hedgehog production. In order to investigate how different experimentally observed mechanisms affect this robustness, we have developed and analysed a new model of Hedgehog gradient formation and signalling. Rather than including every known interaction and reaction rate, our model focuses on the main feedback loops and mechanisms involved in Hedgehog transport and signalling. This allows us to use a combination of numerical simulation of the full model and mathematical analysis of simplified models to better understand the patterning functions associated with these important feedbacks and regulatory mechanisms. Using relatively simple models has also allowed us to provide estimates for model parameters.

An important objective of our modelling work is to build upon the current understanding of the system, by providing (i) a formal description of system that is consistent with data, (ii) functional predictions for important mechanisms and (iii) ways of discriminating between alternative hypotheses that cannot be resolved by classical genetic techniques.

Our principal results predict how the following could enhance robustness to changes in HH levels:

1. Regulation of HH accumulation, transport and stability by HSPGs in posterior cells.

2. 'Self-enhanced' HH internalisation in anterior cells.

Our model predicts that cell surface proteins, such as HSPGs, could enhance robustness by restricting the amount of stable HH that can be held by, and transported across, posterior cells. Once levels of HH reach μ at the posterior margin, any additional HH protein produced in the most posterior cells is degraded rather than being held stably at the surface and transported anteriorly. This in turn leads to smaller variations in HH levels in anterior cells, compared to the scenario when HH can diffuse freely or without local regulation (Fig. 5). These results are interesting when taken in the context of available data on HSPGs. HH accumulation is inhibited by mutations in the HSPG dally (Takeo et al. (2005)), as well as in mutations that modify HSPG activity, such as *shifted*, *tout velu* and *sister of tout velu* (Bornemann et al. (2004), Glise et al. (2005)). Meanwhile, HH movement across the tissue is impeded in cells mutant for both *dally* and *dlp* (double mutant) (Han et al. (2004)), *shifted* (Glise et al. (2005)), *tout velu* and *sister of tout-velu* (Bornemann et al. (2004)). However, to what degree the effects of these different mutations are attributable to changes in HH stability or transport, or in the levels of HH that can be held and/or modulated by HSPG remains to be elucidated. The modelling work presented here predicts that allowing HSPGs to restrict the amount of HH held (via μ) has the most significant effect on robustness and HH gradient formation (see also *Supporting Figure* S4). It is currently difficult to determine whether such a restriction mechanism occurs *in vivo*, since manipulations to HSPGs and related proteins often affect multiple functions. However, the model provides a useful tool for discriminating between the different possibilities and predicts that such a restriction mechanism changes the qualitative behaviour of the system. From Fig. 5B and *Supporting Figure* S4, we see that the transition to a robust phase is dependent on this restriction mechanism, and cannot be observed when only HSPG-regulated transport and stability are taken into account. Moreover, the qualitative nature of the increase in HH levels at the AP boundary differs—between straight/convex (red line) and concave (black dashed line)—only once the restriction mechanism (via μ) is taken into account. Support for such a restriction mechanism could be obtained by experimentally mimicking Fig. 5B, for instance by recording the expression range of HH targets and/or HH levels at the AP boundary in response to different rates of Hedgehog production.

Our second area of investigation focused on the anterior signalling pathway and how the regula-

tion of HH-PTC internalisation could enhance robustness to changes in HH levels. In particular, we found that any of the following could enhance robustness:

(2a) Up-regulation of *ptc* in response to Hedgehog signalling,

(2b) Antagonism of PTC by the HH-PTC complex,

(2c) Increased HH-PTC binding and internalisation close to the AP boundary (due to HSPG up-regulation),

(2d) Decreased HH diffusion rate close to the AP boundary,

(2e) Positive feedback between SMO and FU within the signalling pathway.

Previous studies (e.g. Eldar et al. (2003)) have demonstrated how regulation of receptor levels by signalling could enhance robustness to changes in morphogen level by increasing morphogen degradation rates in response to signalling (e.g. (a) above). Our findings are an extension of this 'self enhanced degradation' mechanism since including (a)–(e) in our model all result in an increase in the total amount of HH-PTC internalised and degraded close to the AP boundary. Mechanisms (b), (c) and (e) are positive feedbacks that antagonise the negative feedback up-regulating PTC (Fig. 2). This leads to more PTC and a steeper HH gradient close to the AP boundary, giving a consequent enhancement of positional robustness beyond that resulting from mechanism (a) alone (Fig. 4A and Fig. 6). These results suggest functional roles for a number of experimentally observed mechanisms. For example, mechanism (c) suggests a function for the HSPG Dally-like in robustness. Experimental evidence shows that Dally-like is up-regulated in response to Hedgehog signalling, as well as being co-internalised with the HH-PTC complex to promote signalling (Gallet et al. (2008)). Mechanism (d) is also interesting in the context of Shh signalling in vertebrates, where the signalling target Hhip1 sequesters Shh at the cell surface (Chuang and McMahon (1999)). This ability to increase robustness through reduced diffusion has also been proposed by other authors (Bollenbach et al. (2007)).

The inclusion of regulated transport and regulative feedback in our models provides a better fit to experimental data on the shape of the Hedgehog gradient. One fact that is apparent from these data is that posterior HH levels are not significantly higher than levels at the AP boundary (up to a 2-fold change seems reasonable: Tabata and Takei (2004), Eugster et al. (2007)). However, in the free diffusion models (Model A in *Supporting Text*, when $D_b(A) = D_b(P)$) this ratio is

$$\beta = 1 + \frac{\lambda_P}{\lambda_A}\left(\frac{1}{\tanh\dfrac{L_P}{\lambda_P}}\left(1 - \frac{1}{\cosh\dfrac{L_P}{\lambda_P}}\right)\right), \tag{16}$$

which is less than 2 only when $\gamma(A) < \gamma(P)$. This would then imply that HH would have to be degraded faster in the posterior compartment, which is not believed to be the case. However, the inclusion of HSPGs in the model provides a number of additional ways of matching model behaviour to the observed data. In this case,

$$\beta = \frac{1}{2} + \sqrt{\frac{1}{4} + \frac{\mu D_b(A)^2}{2\rho_h \lambda_A^2 D_b(P)}}. \tag{17}$$

Allowing HSPGs to modulate diffusion rates D_b and/or limit the amount of HH that can be held at the surface (μ), can give the desired result. Furthermore, a positive feedback of some sort—such as HH-PTC antagonism of PTC function (mechanism (2b)) or HSPG up-regulation in response to signalling (mechanism 2(c))—is required to provide a good qualitative fit with the available experimental data. Expression data show that PTC protein is expressed at a high level in four to five anterior compartment cells adjacent to the compartment boundary, followed by a sharp drop off (Glise et al. (2002), Casali and Struhl (2004)). In the model containing only the negative feedback loop, we observe a shallow PTC gradient, since PTC up-regulation is limited by its own levels (see blue line in Fig. 4). However, once either of the two positive feedbacks are taken into account, the sharp PTC gradient observed in the data begins to emerge.

The available experimental data (such as that discussed above) also allow us to constrain the values of a number of the parameters in our non-dimensionalised model (see Table 1 and constraints **C1**–**C10** in *Supporting Text*). Non-dimensionalisation is achieved by expressing parameters in terms of basal production and degradation rates of PTC (ρ_{p1}, γ_p) and the average cell size $w \approx 2.6\mu m$ (Kicheva et al. (2007)). Previous modelling studies have used $\gamma_p = 0.0015s^{-1}$ (Lai et al. (2004), Saha and Schaffer (2006), Nahmad et al. (2008)), based on measurements for the EGF pathway (French and Lauffenburger (1996)), or $\gamma_p = 0.000625s^{-1}$ (Eldar et al. (2003)). In our model, these values would lead to diffusion rates of D_b of 0.6084 and 0.2535 $\mu m^2 s^{-1}$, respectively. However, these parameter values would lead to faster gradient formation than is observed in the wing disc (approximately 24 hours—Su et al. (2007)). Setting $\gamma_p = 0.0001s^{-1}$ gives a more feasible time-scale for the establishment of the gradient, and gives a diffusion rate

of $D_b = 0.04\mu m^2 s^{-1}$, which is comparable to that observed for Decapentaplegic (0.1 $\mu m^2 s^{-1}$) and Wingless (0.05 $\mu m^2 s^{-1}$) in the wing disc (Kicheva et al. (2007)).

In our models, it is necessary to assign values to the following parameters (with each concentration scaled by PTC levels at the anterior margin)

1. $z_A = \dfrac{[PTC]}{1 + r[PH]}$ at the boundary of high PTC production,
2. μ, the stable HH concentration at the posterior margin,
3. α_0, the stable HH concentration at the AP boundary.

These values could be determined from accurate measurements of (relative) levels of HH, PTC and HH-PTC across the disc. To the best of our knowledge, these experimental data do not exist, and so these measurements would be most valuable for future parameter estimation. In making this point, we are assuming that most HH is bound to HSPG and that the remainder degrades rapidly. Therefore, any experiment that could determine the relative levels of bound and free HH types would also assist parameter estimation.

The focus of this paper has been robustness to variations in Hedgehog levels. However, our models also suggest potential trade-offs between robustness and additional features of the Hedgehog gradient, such as signalling range and size regulation. For example, restricting the amount of stable HH at the cell surface results in the insensitivity of the HH gradient to changes in disc size. Once the size of the posterior compartment L_P surpasses the threshold x_P, the anterior gradient remains unchanged (note that L_P has no effect on Eqn. (10)). Therefore, if HH target expression boundaries scale with disc size this may be mediated through regulated growth downstream of HH, rather than through the HH gradient itself changing. We also observe a trade-off between robustness and signalling range when considering feedback within the anterior signalling pathway. This is because enhanced HH binding/degradation near the AP boundary leads to a steeper gradient and lower HH levels away from the boundary (Fig. 4A). In relation to this trade off, regulation of HH diffusion, HH-PTC internalisation rate, or the strength of HH-PTC antagonism of the repression of SMO activity by PTC, can provide a way of balancing robustness with signalling range. If the HH-PTC internalisation (or HH diffusion) rate is changed uniformly across the tissue then any enhanced robustness is counteracted by a more dramatic decrease in signalling range, compared to the models incorporating differential regulation of these properties

(e.g. blue vs red and black dashed lines in *Supporting Figure* S1D). This advantage resulting from differential regulation of Hedgehog transport/internalisation across the gradient is particularly interesting when we consider the Shh gradient and cell surface proteins in the vertebrate neural tube (Dessaud et al. (2008)). Here, Hedgehog-interacting protein (Hhip) is up-regulated in response to high levels of signalling, leading to a greater amount of Shh being held near the source and effectively reducing the rate of transport across the tissue. Meanwhile, other cell surface proteins such as Gas1, Cdo and Boc are only expressed at low levels of signalling (due to inhibition by Shh signalling) but enhance signalling efficiency.

In order to allow mathematical analysis, a number of simplifications were incorporated in our models. Therefore, there are a number of ways in which our model could be developed and improved in the future. In our model the effects of SMO, FU, COS2, CIA and CIR are simplified into a single variable S. Representing these with separate variables would allow us to analyse signalling properties in more detail. Moreover, additional feedbacks have been observed within the signalling pathway. For example, Engrailed and Roadkill are both up-regulated in response to the highest levels of signalling, and down-regulate CI (Eaton and Kornberg (1990), Strigini and Cohen (1997), Kent et al. (2006)). However, we note that in the case of Roadkill, PTC production and patterning are not radically affected (Kent et al. (2006)). In the current version of our model, we have assumed that secretion and transport rates are uniform across all posterior cells and not dependent on the precise concentrations of important proteins such as Dispatched, Shifted, Dally and Dally-like. However, there are some spatial variations in the expression levels of these proteins that could be examined in future models. For example, Dally-like is expressed at low levels in all posterior cells (Gallet et al. (2008)), whilst Dally is expressed at low levels in posterior cells near the border and higher levels at the margins (Crickmore and Mann (2007)). Moreover, both Dally and Dally-like are up-regulated in a stripe in anterior cells near the anterior-posterior border (Fujise et al. (2001), Crickmore and Mann (2007), Gallet et al. (2008)). A number of additional secretion / transport mechanisms could be added to future models. In particular, HH secretion, HH signalling, HH transport and HH-HSPG interactions have been shown to be affected by HH lipid modifications (Callejo et al. (2006)). Interestingly these modifications also determine whether HH is transported across the apical or basolateral surface of the wing disc epithelium. Adding variables for mRNAs and adding time delays to processes such as transcription and translation could also make the models more realistic and allow us to study the dynamics of gradient formation in greater detail (as opposed to the steady

state gradients which have been the focus of this paper). Considering the duration as well as the strength of signalling on targets such as *dpp* (Nahmad and Stathopoulos (2009)) would also be a fruitful area of further research. Finally, it would also be of interest to adapt the model to more closely represent Shh signalling, particularly by including a number of Shh-regulated cell surface proteins that affect morphogen transport and signalling.

Acknowledgements

We thank Yogi Jaeger for helpful comments on the manuscript. D.I and N.M are supported by EPSRC grant EP/D003105/1. A.W. and B.G. are supported by grants from the "Agence Nationale pour la Recherche" (ANR), the Université Paul-Sabatier, CNRS and "Association pour la recherche sur la sclérose en plaques" (ARSEP). A.W. is supported by a graduate fellowship from the French "Ministère de l'enseignement supérieur et de la recherche".

References

Affolter, M., Basler, K., 2007. The decapentaplegic morphogen gradient: from pattern formation to growth regulation. Nat. Rev. Genet. 8, 663–674.

Ashe, H., Briscoe, J., 2006. The interpretation of morphogen gradients. Development 133, 385–394.

Basler, K., Struhl, G., 1994. Compartment boundaries and the control of drosophila limb pattern by hedgehog protein. Nature 368, 208–214.

Ben-Zvi, D., Shilo, B., Fainsod, A., Barkai, N., 2008. Scaling of the bmp activation gradient in xenopus embryos. Nature 453, 1205–1211.

Blair, S., 2007. Wing vein patterning in drosophila and the analysis of intercellular signaling. Annu. Rev. Cell Dev. Biol. 23, 293–319.

Bollenbach, T., Kruse, K., Pantazis, P., González-Gaitán, M., Jülicher, F., 2007. Morphogen transport in epithelia. Phys. Rev. E 75, 011901.

Bornemann, D., Duncan, J., Staatz, W., Selleck, S., Warrior, R., 2004. Abrogation of heparan sulfate synthesis in *drosophila* disrupts the wingless, hedgehog and decapentaplegic signaling pathways. Development 131, 1927–1938.

Callejo, A., Torroja, C., Quijada, L., Guerrero, I., 2006. Hedgehog lipid modifications are required for hedgehog stabilization in the extracellular matrix. Development 133, 471–483.

Casali, A., Struhl, G., 2004. Reading the hedgehog morphogen gradient by measuring the ratio of bound to unbound patched protein. Nature 431, 76–80.

Chen, Y., Struhl, G., 1996. Dual roles for patched in sequestering and transducing hedgehog. Cell 87, 553–563.

Chuang, P., McMahon, A., 1999. Vertebrate hedgehog signalling modulated by induction of a hedgehog-binding protein. Nature 397, 617–621.

Claret, S., Sanial, M., Plessis, A., 2007. Evidence of a novel feedback loop in the hedgehog pathway involving smoothened and fused. Curr. Biol. 17, 1326–1333.

Crickmore, M., Mann, R., 2007. Hox control of morphogen mobility and organ development through regulation of glypican expression. Development 134, 327–334.

Crozatier, M., Glise, B., Khemici, V., Vincent, A., 2003. Vein-positioning in the drosophila wing in response to hh; new roles of notch signaling. Mech. Dev. 120, 529–535.

Crozatier, M., Glise, B., Vincent, A., 2002. Connecting hh, dpp and egf signalling in patterning of the drosophila wing; the pivotal role of collier/knot in the ap organiser. Development 129, 4261–4269.

Dessaud, E., McMahon, A., Briscoe, J., 2008. Pattern formation in the vertebrate neural tube: a sonic hedgehog morphogen-regulated transcriptional network. Development 135, 2489–2503.

Dillon, R., Gadgil, C., Othmer, H., 2003. Short- and long-range effects of sonic hedgehog in limb development. Proc Natl Acad Sci U S A 100, 10152–10157.

Dubois, L., Enriquez, J., Daburon, V., Crozet, F., Lebreton, G., Crozatier, M., Vincent, A., 2007. Collier transcription in a single drosophila muscle lineage: the combinatorial control of muscle identity. Development 134, 4347–4355.

Eaton, S., Kornberg, T., 1990. Repression of ci-d in posterior compartments of drosophila by engrailed. Genes & Dev 4, 1068–1077.

Eldar, A., Rosin, D., Shilo, B., Barkai, N., 2003. Self-enhanced ligand degradation underlies robustness of morphogen gradients. Dev. Cell 5, 635–646.

Eugster, C., Pánaková, D., Mahmoud, A., Eaton, S., 2007. Lipoprotein-heparan sulfate interactions in the hh pathway. Dev. Cell 13, 57–71.

French, A., Lauffenburger, D., 1996. Intracellular receptor / ligand sorting based on endosomal retention components. Biotech. Bioeng. 51, 281–297.

Fujise, M., Izumi, S., Selleck, S., Nakato, H., 2001. Regulation of *dally*, and integral membrane proteoglycan, and its function during adult sensory organ formation of *drosophila*. Dev. Biol. 235, 433–448.

Gallet, A., Staccini-Lavenant, L., Thérond, P., 2008. Cellular trafficking of the glypican dally-like is required for full-strength hedgehog signaling and wingless transcytosis. Dev. Cell 14, 712–725.

Glise, B., Jones, D., Ingham, P., 2002. Notch and wingless modulate the response of cells to hedgehog signalling in the drosophila wing. Dev. Biol. 248, 93–106.

Glise, B., Miller, C., Crozatier, M., Halbisen, M., Wise, S., Olson, D., Vincent, A., Blair, S., 2005. Shifted, the drosophila ortholog of wnt inhibitory factor-1, controls the distribution and movement of hedgehog. Dev. Cell 8, 255–266.

González, A., Chaouiya, C., Thieffry, D., 2008. Logical modelling of the role of the hh pathway in the patterning of the *drosophila* wing disc. Bioinformatics 24 (ECCB 2008), i234–i240.

Han, C., Belenkaya, T., Wang, B., Lin, X., 2004. *Drosophila* glypicans control the cell-to-cell movement of hedgehog by a dynamin-independent process. Development 131, 601–611.

Hufnagel, L., Kreuger, J., Cohen, S. M., Shraiman, B. I., 2006. On the role of glypicans in the process of morphogen gradient formation. Dev. Biol. 300, 512–522.

Ingham, P., McMahon, A., 2001. Hedgehog signalling in animal development: paradigms and principles. Genes & Dev. 15, 3059–3087.

Jaeger, J., Irons, D., Monk, N., 2008. Regulative feedback in pattern formation: towards a general relativistic theory of positional information. Development 135, 3175–3183.

Jia, J., Jiang, J., 2006. Decoding the hedgehog signal in animal development. Cell. Mol. Life Sci. 63, 1249–1265.

Jiang, J., Hui, C., 2008. Hedgehog signaling in development and cancer. Dev. Cell 15, 801–812.

Kent, D., Bush, E., Hopper, J., 2006. Roadkill attenuates hedgehog responses through degradation of cubitus interruptus. Development 133, 2001–2010.

Kicheva, A., Pantazis, P., Bollenbach, T., Kalaidzidis, Y., Bittig, T., González-Gaitán, F. J. M., 2007. Kinetics of morphogen gradient formation. Science 315, 521–525.

Lai, K., Robertson, M., Schaffer, D., 2004. The sonic hedgehog signaling system as a bistable genetic switch. Biophys. J. 86, 2748–2757.

Lander, A., 2007. Morpheus unbound: Reimagining the morphogen gradient. Cell 128, 245–256.

Lander, A., Nie, Q., Wan, F., 2002. Do morphogen gradients arise by diffusion? Dev. Cell 2, 785–796.

Lander, A., Nie, Q., Wan, F., 2007. Membrane-associated non-receptors and morphogen gradients. Bull. Math. Biol. 69, 33–54.

Lee, J., von Kessler, D. P., Parks, S., Beachy, P. A., 1992. Secretion and localized transcription suggest a role in positional signaling for products of the segmentation gene hedgehog. Cell 71, 33–50.

Lin, X., 2004. Functions of heparan sulfate proteoglycans in cell signaling during development. Development 131, 6009–6021.

Liu, Y., Cao, X., Jiang, J., Jia, J., 2007. Fused-costal2 protein complex regulates hedgehog-induced smo phosphorylation and cell-surface accumulation. Genes & Dev 21, 1949–1963.

Marigo, V., Tabin, C., 1996. Regulation of patched by sonic hedgehog in the developing neural tube. Proc. Natl. Acad. Sci. USA 93, 9346–9351.

Mullor, J., Sánchez, P., Ruiz i Altaba, A., 2002. Pathways and consequences: Hedgehog signaling in human disease. Trends Cell Biol. 12, 562–569.

Nahmad, M., Glass, L., Abouheif, E., 2008. The dynamics of developmental system drift in the gene network underlying wing polyphenism in ants: a mathematical model. Evo. & Dev. 10, 360–374.

Nahmad, M., Stathopoulos, A., 2009. Dynamic interpretation of hedgehog signalling in the drosophila wing disc. PLoS Biol. 7, e1000202.

Saha, K., Schaffer, D., 2006. Signal dynamics in sonic hedgehog tissue patterning. Development 133, 889–900.

Slusarski, D., Motzny, C., Holmgren, R., 1995. Mutations that alter the timing and pattern of cubitus interruptus gene expression in drosophila melanogaster. Genetics 139, 229–240.

Strigini, M., Cohen, S., 1997. A hedgehog activity gradient contributes to ap axial patterning of the drosophila wing. Development 124, 4697–4705.

Su, V., Jones, K., Brodsky, M., The, I., 2007. Quantitative analysis of hedgehog gradient formation using an inducible expression system. BMC Dev. Biol. 7, 43.

Tabata, T., Takei, Y., 2004. Morphogens, their identification and regulation. Development 131, 703–712.

Takeo, S., Akiyama, T., Firkus, C., Aigaki, T., Nakato, H., 2005. Expression of a secreted form of dally, a drosophila glypican, induces overgrowth phenotype by affecting action range of hedgehog. Dev. Biol. 284, 204–218.

Umulis, D., Serpe, M., O'Connor, M., Othmer, H., 2006. Robust, bistable patterning of the dorsal surface of the drosophila embryo. Proc. Natl. Acad. Sci. USA 103, 11613–11618.

Varjosalo, M., Taipale, J., 2008. Hedgehog: functions and mechanisms. Genes & Dev. 22, 2454–2472.

Tables

Table 1: Default parameter set for the non-dimensionalised model, which satisfy the constraints **C1**–**C10** described in *Supporting Text*. Values and landmark positions (see Fig.1) are also listed, along with Equations giving approximations

Variable	Description	Default value	Constraint used
ρ_h	Hedgehog production rate	30	**C10**
ρ_{p1}	Basal Patched production rate	1	By non-dimenisionalisation
ρ_{p2}	Transcriptional Patched production rate	36	**C8**
γ_f	Free HH (HH_f) degradation rate	6	**C5**
γ_b	Bound HH-HSPG (HH_b) degradation rate	0.01	**C3**
γ_p	PTC degradation rate	1	By non-dimenisionalisation
γ_{ph}	HH-PTC degradation rate	6	**C4**
D_f	Free HH (HH_f) transport rate	0.6	**C6**
D_b	Bound HH-HSPG (HH_b) transport rate	60	**C9**
k_{on}	HH-PTC binding & internalisation rate	8	**C9**
k_{off}	HH-PTC unbinding rate	0.01	**C2**
k_{out}	HH-HSPG binding rate	10	(estimate)
k_{in}	HH-HSPG unbinding rate	0.01	**C1**
μ	HH-HSPG saturation level	20	(estimate)
r	PTC antagonism (by HH-PTC)	0.8	**C7**
L_A	Anterior compartment width	40 cells	(estimate)
L_P	Posterior compartment width	40 cells	(estimate)
z_A	Level of $[Z]$ corresponding to the *ptc* production threshold	0.3	(estimate)
c_p	Threshold for *ptc* up-regulation	0.76	c_p,c_s and n_s ensure $z_A = 0.3$
c_s	Threshold for signalling (S) up-regulation	0.4	
n_p	Hill coefficient for PTC up-regulation	8	
n_s	Hill coefficient for signalling (S) up-regulation	4	
δ	Approximation of $[PTC]$ away from high *ptc* production region	0.6	(estimate)
α_0	HH_b level at the AP boundary	Eqn 10	
α_A	HH_b level at the Patched production boundary	Eqn 13	
$[HH_b]_T$	HH_b level at (generic) target gene boundary		
g	Magnitude of HH_b gradient at AP boundary	Eqn 15	
β	Ratio between HH_b at the posterior margin and AP boundary	Eqn 17	
x_P	Boundary corresponding to HH-HSPG saturation	Eqn 11	
x_A	Boundary corresponding to high Patched up-regulation	Eqn 14	
x_T	Boundary corresponding to (generic) target gene	Eqn 12	

Table 2: High Patched response threshold (α_A) and magnitude of gradient (Eqn. (15)) for different parameter sets described in Fig. 4, and default parameters in Table 1. We also include an additional case including all three feedbacks. $\star$: In the case where $\alpha_A > \alpha_0$ and $r = 0$, $[PTC]$ approaches $z_A = 0.3$ near the AP boundary and this affects the approximation δ. We therefore show the gradient for $\delta = 0.3$ (2) and $\delta = 0.6$ (2.82). The default value of $\delta = 0.6$ is used for the remaining parameter sets.

ρ_{p2}	r	k_{on} (high)	α_A	gradient when $\alpha_0 = 10$
36	0	8	15.32	2.0 – 2.82 *
36	0.8	8	2.58	3.11
36	0	40	3.06	3.05
36	0.8	40	0.52	3.42

Figures

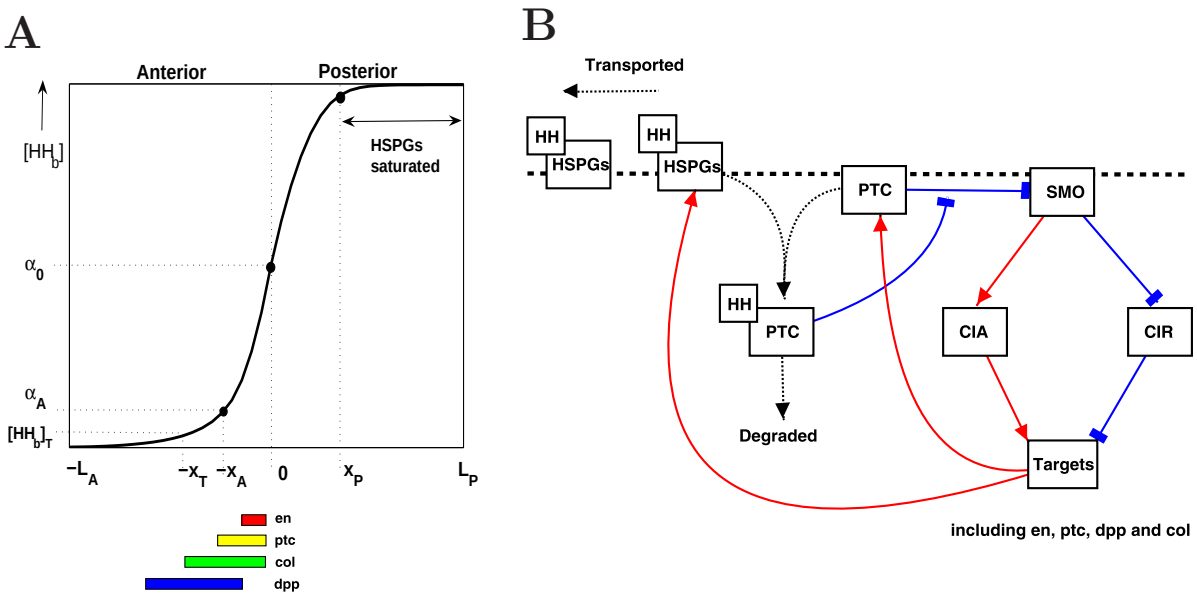

Figure 1: Summary of Hedgehog gradient formation and signalling. (A) Hedgehog is produced in all posterior cells (right) and travels anteriorly (left), forming a concentration gradient. Target genes, including *en*, *ptc*, *col* and *dpp*, then respond in a concentration dependent manner. Late 3rd instar wing disc patterns are shown. Concentrations and boundaries of interest are marked and described in Table 1, along with equation numbers (where appropriate). (B) Main interactions involved in Hedgehog signalling, in anterior cells. Red arrows and blue bars correspond to activation and inhibition, respectively. Dashed arrows correspond to binding, internalisation and degradation. See main text for discussion.

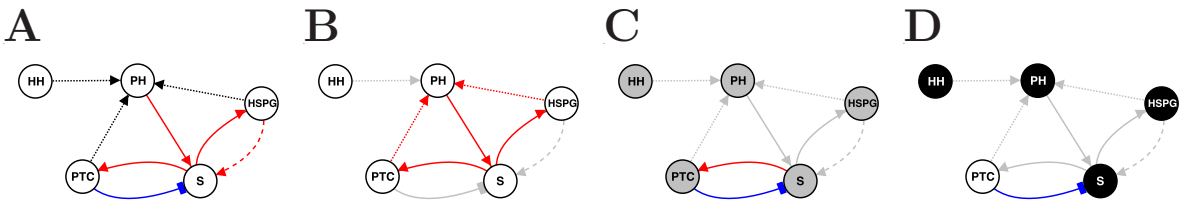

Figure 2: (A) Summary of the main interactions included the model. S corresponds to a generic 'signalling response' variable corresponding to SMO and CI activity. PH corresponds to the HH-PTC complex. (B-D) Dominant feedbacks loops and interactions in response to high (white), medium (grey) and low (black) levels of HH.

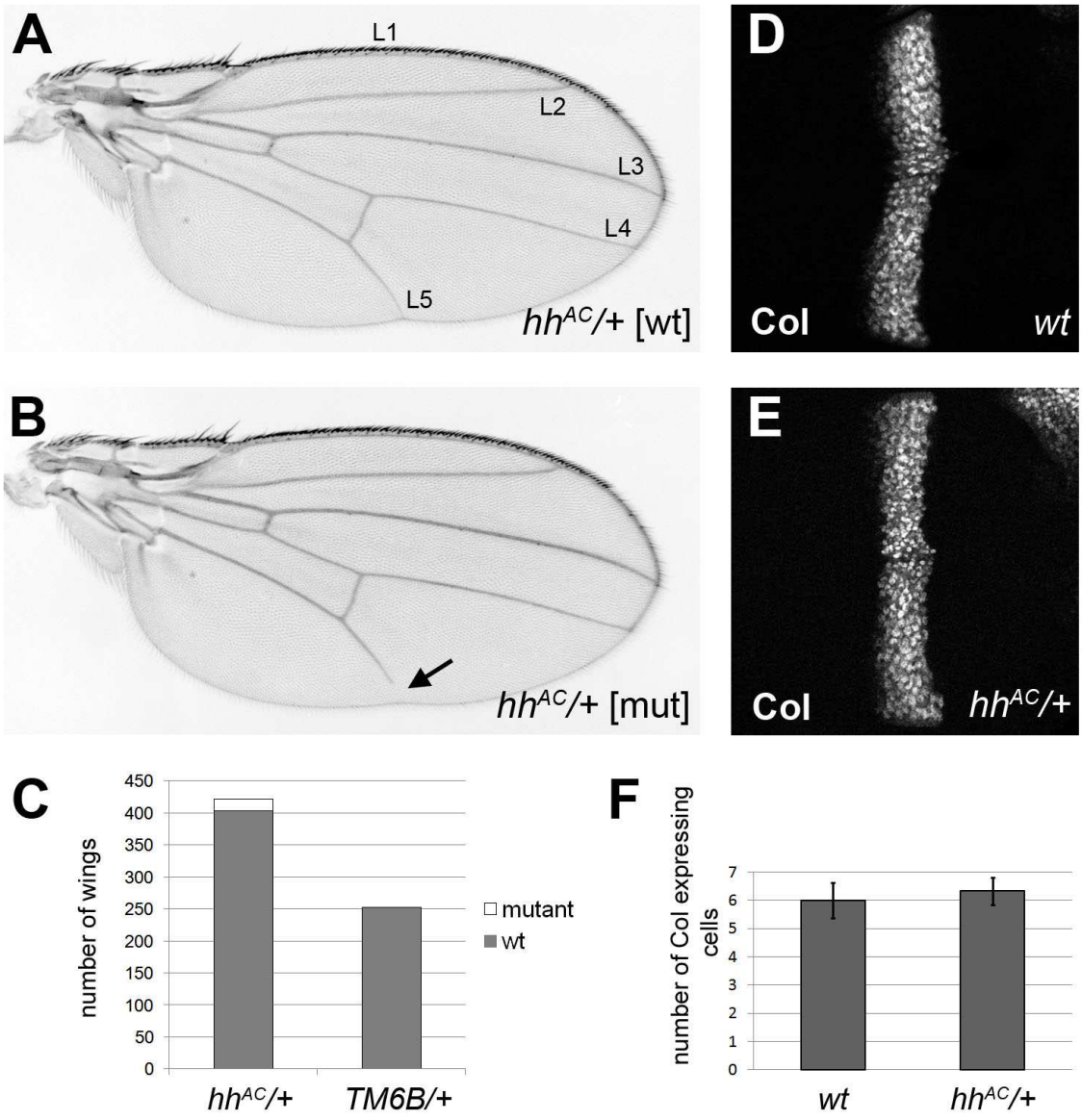

Figure 3: Robustness of Hedgehog patterning during wing development. (A-B) Adult wing phenotypes from hh^{AC}/+ flies. (A) 95% of the wings present a wild-type phenotype [wt] with, in particular, the correct positioning of the longitudinal veins (L1 to L5). (B) The remaining 5% of the wings show a consistent disruption of the tip of L5 vein (arrow) with no other visible defects. (C) Analysis of all wings from adults emerging from the cross of hh^{AC}/TM6B with wild-type flies were analysed. All TM6B/+ wings (n=252) were *wt* and of all the hh^{AC}/+ wings analysed (n=422), around 5% of the wings (n=19) present the characteristic phenotype presented in panel B. (D–E) Collier (Col) expression pattern in hh^{AC}/+ late third instar wing imaginal disc compared to wild-type. The discs are oriented anterior to the left, posterior to the right, dorsal up and ventral down. (F) Analysis of the number of cells activating, in the anterior compartment, Collier expression in *wt* and hh^{AC}/+ discs. In both backgrounds, Collier is expressed in a stripe of width 6 cells along the AP axis.

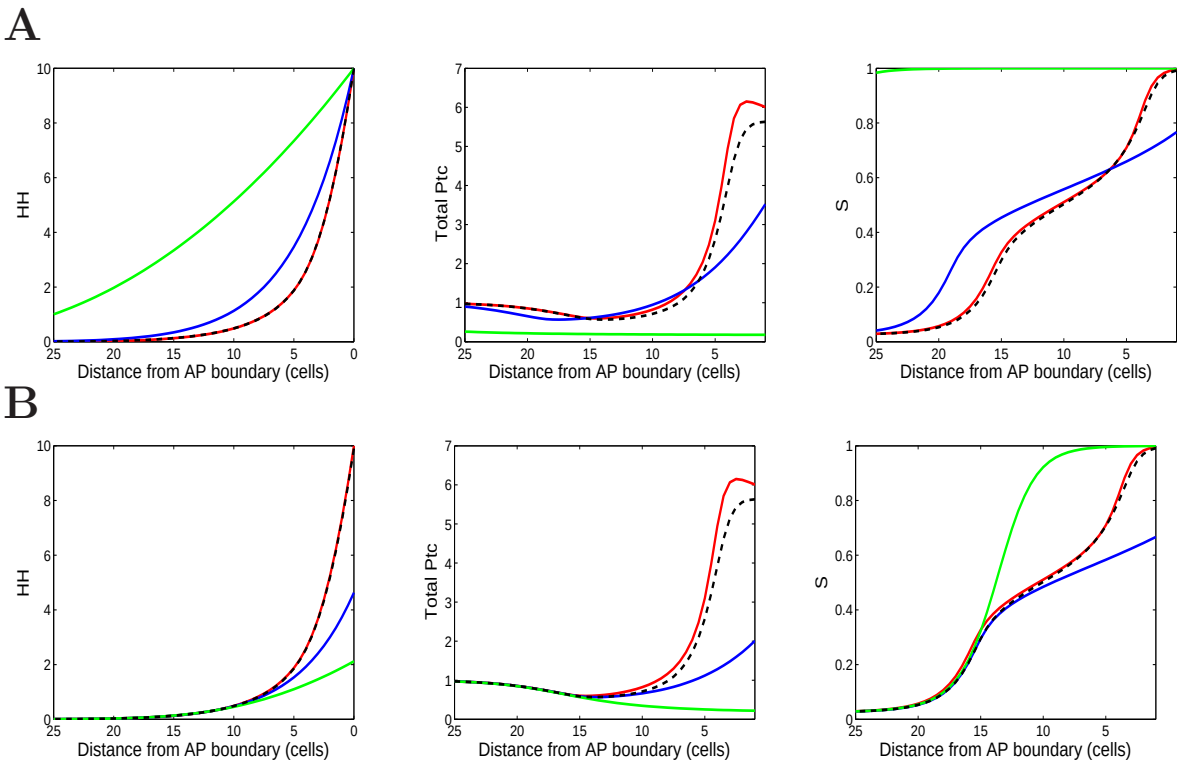

Figure 4: Anterior HH ($[HH_b]$), PTC ($[PTC] + [PH]$) and S gradients for different parameter sets. In all cases, HH_b levels at the AP boundary (α_0) are fixed and Eqns. (3)–(8) are used to simulate gradient formation. Default parameters are taken from Table 1 but differ in the 4 cases as follows. Green: $r = 0$, $\rho_{p2} = 0$; Blue: $r = 0$, $\rho_{p2} = 36$; Red: $r = 0.8$, $\rho_{p2} = 36$; Black Dashed line corresponds to the case where $r = 0$, $\rho_{p2} = 36$, and k_{on} increases 5-fold in response to high Hedgehog signalling. (A) $\alpha_0 = 10$ in each case, (B) α_0 varies in each case to ensure HH_b levels are equal at 12 cells

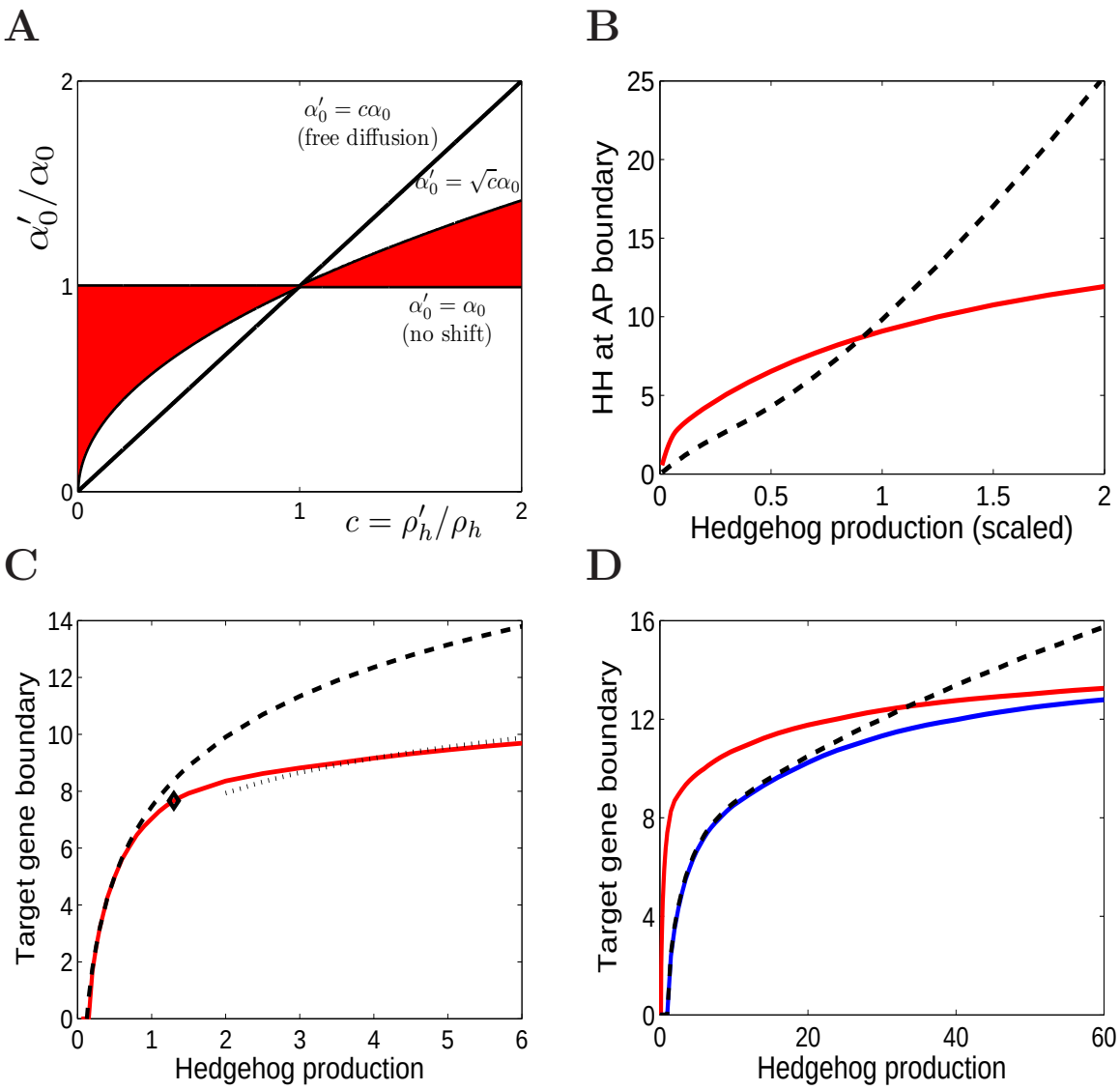

Figure 5: (A) Bounds on gradient shifts for the case $x_P < L_P$ (when HSPGs become saturated by HH at the posterior margin). The possible range for shifts in HH levels at AP boundary (α_0), in response to a c-fold change in Hedgehog production rate (ρ_h) corresponds to the shaded region. Lines for 'free diffusion' and 'no shift' cases are given for comparison. (B) Simulations for shifts in HH levels at the AP boundary for the default model (red) and the free diffusion model (black dashed line). (C) Shift in target gene boundary in response to changes in HH production for the default model (red). Black dashed lines correspond to theoretical predictions for the free diffusion model, whilst the dotted line corresponds to the outer bound of the regulated transport case ($\sqrt{c}$ case in A). The diamond indicates the threshold ($x_P = L_P$) separating the two behaviours. (D) Direct comparison of the full model with different parameter sets. Red: Default parameters from Table 1; Blue: $\gamma_b = 1$; Black dashed: $\gamma_b = 1$, $\mu = 2000$ (equivalent to free diffusion).

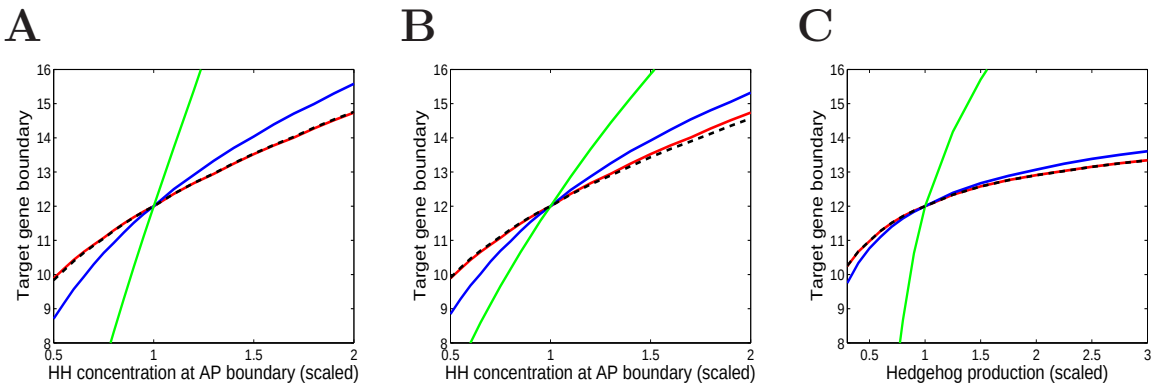

Figure 6: (A,B) Shift in target gene boundary in response to changes in HH levels at the AP boundary (α_0), for the parameter sets and base values of α_0 given in Fig. 4A and B respectively. In each case, the HH concentration at 12 cells (when α_0 is at its base value), is used to define and track the target gene boundary. (C) Shift in target gene boundary in response to changes in Hedgehog production (ρ_h) for the full anterior-posterior model, for the parameter sets and base values of ρ_h given in Fig. 4 and *Supporting Figure* S2B. The HH concentration at 12 cells (when ρ_h is at its base value), is used to define and track the target gene boundary.

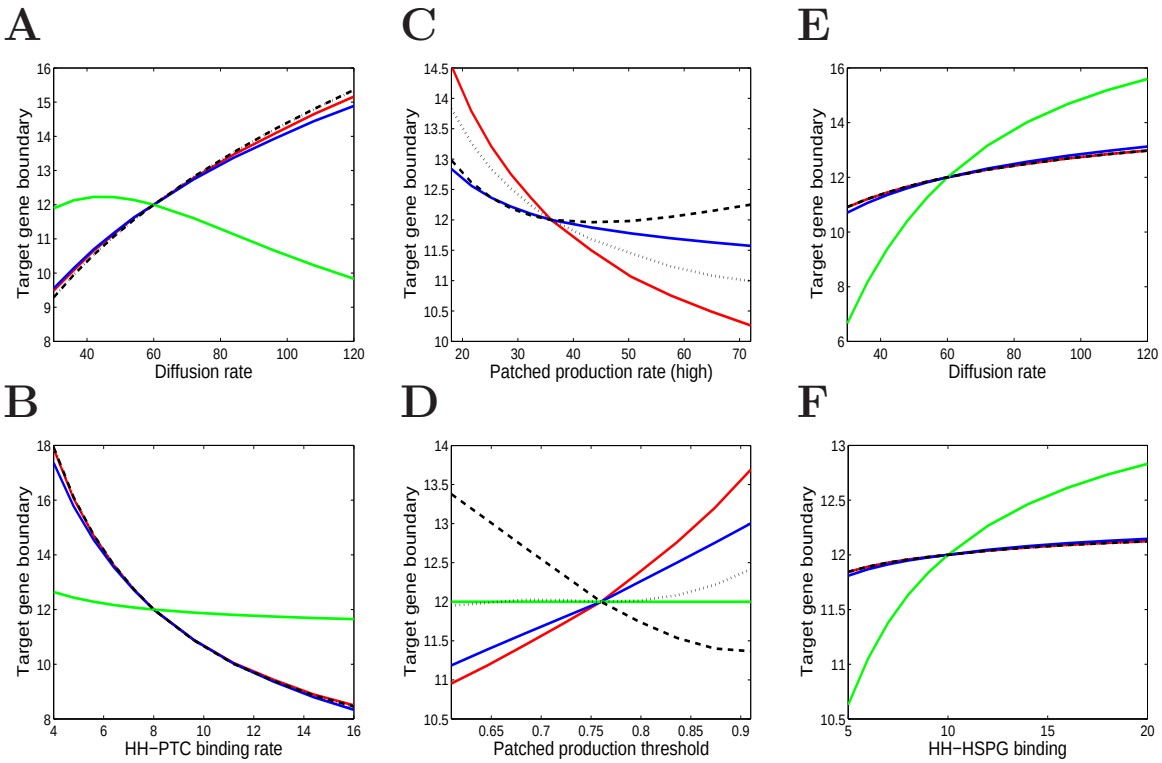

Figure 7: Shift in target gene boundary in response to parameter changes. Here, we use the full anterior-posterior model, along with the parameter sets and base values of ρ_h given in Fig. 4 and *Supporting Figure* S2B. In addition, the black dotted line corresponds to the case where r = 0.4 and k_{on} is increased 3.6-fold in response to signalling (mix of red and black dashed case). Target gene boundaries correspond to the HH concentration at 12 cells, when the parameter in question is at its default value (in Table 1) and ρ_h takes its base value. (A–D) Anterior changes to $D_b(A)$, k_{on}, ρ_{p2} and c_p, respectively. (E,F) Posterior changes to $D_b(P)$ and k_{out}, respectively.